

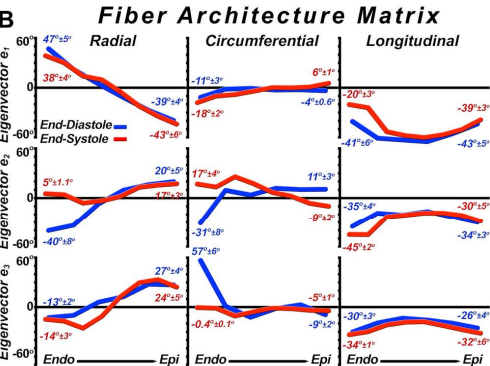
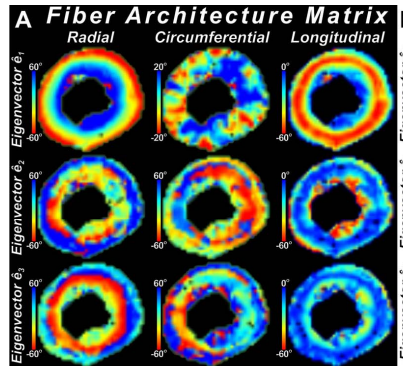
Dynamics of the Fiber Architecture Matrix in the Human Heart *In Vivo*

Choukri Mekkaoui¹, Sonia Nielles-Vallespin², Marcel Jackowski³, Timothy Reese⁴, Peter Gatehouse², David Firmin⁵, and David Sosnovik⁴

¹Harvard Medical School - Massachusetts General Hospital - Athinoula A Martinos center for Biomedical, Boston, MA, United States, ²CMR Unit, Royal Brompton Hospital, London, London, United Kingdom, ³University of São Paulo, São Paulo, São Paulo, Brazil, ⁴Harvard Medical School - Massachusetts General Hospital - Athinoula A Martinos center for Biomedical, Charlestown, MA, United States, ⁵CMR Unit, Royal Brompton Hospital, London, London, United States

Target Audience: Scientists interested in the application of diffusion tensor MRI in the heart.

Purpose: *In vivo* Diffusion Tensor MRI (DTI) of the human heart has shown that myofiber architecture is dynamic as the left ventricle (LV) contracts and relaxes.¹ However, most architecture-related information derived from the diffusion tensor, such as the helix angle (HA),² and the more recent tractographic propagation angle (PA),³ have relied solely upon information from the principal eigenvector. Here, we introduce the fiber architecture matrix (FAM), which is a function of the complete tensor eigensystem, to aid in the characterization of myofiber dynamics *in vivo*. The FAM encodes myofiber architecture by the projections of all three eigenvectors with respect to the three orthogonal planes (radial, circumferential, and longitudinal) that represent the cardiac coordinate system.



Methods: DTI of 10 normal volunteers was performed on a 3T clinical scanner (Skyra, Siemens) with the following parameters: 6 diffusion-encoding directions, $b=350\text{s/mm}^2$, fat saturation, $TR/TE=1100/23\text{ms}$, $BW=2442\text{Hz/pixel}$, spatial resolution= $2.7\times 2.7\times 8\text{mm}^3$, 8 averages. This required 24 separate breatholds for a 3-slice diffusion-encoded volume. A local cardiac coordinate system comprising radial (R), circumferential (C), and longitudinal (L) axes was created at each voxel within the myocardium assuming the geometry of the LV. This was accomplished by determining the Euclidean distance map from the epicardial surface using a planar wave propagation technique.⁴ The gradient vector of the distance map determines the R axis, and the two complementary vectors represent the C and L axes. The FAM consists of 9 coefficients, represented by the angles between projections of eigenvectors \hat{e}_1 , \hat{e}_2 , and \hat{e}_3 with respect to the planes defined by the R, C, and L axes, as follows: $FAM = [\langle R, \text{proj}_{\hat{e}_1} R \rangle, \langle C, \text{proj}_{\hat{e}_1} C \rangle, \langle L, \text{proj}_{\hat{e}_1} L \rangle; \langle R, \text{proj}_{\hat{e}_2} R \rangle, \langle C, \text{proj}_{\hat{e}_2} C \rangle, \langle L, \text{proj}_{\hat{e}_2} L \rangle; \langle R, \text{proj}_{\hat{e}_3} R \rangle, \langle C, \text{proj}_{\hat{e}_3} C \rangle, \langle L, \text{proj}_{\hat{e}_3} L \rangle]^T$. The FAM describes fiber architecture based on a local coordinate system that is a function of LV morphology.

Figure 1. (A) The fiber architecture matrix (FAM) is derived from the projections of the three eigenvectors of the diffusion tensor onto the radial (R), circumferential (C) and longitudinal (L) planes of the heart. This produces a second order matrix, with independent and complementary information in each coefficient. $\hat{e}_1 R$, for instance, defines the fiber helix angle and $\hat{e}_2 R$ the sheet angle. 2D maps of fiber architecture created here in a short axis slice at the midventricular level, and 3D tracts can be constructed from any of the FAM coefficients. (B) Translational gradients in the LV, from endocardium to epicardium, of the 9 matrix coefficients. End-diastolic gradients are plotted in blue and end-systolic gradient in red. The greatest changes in systole involve the matrix coefficients describing sheet geometry $\langle R, \text{proj}_{\hat{e}_2} R \rangle$, $\langle C, \text{proj}_{\hat{e}_2} C \rangle$, and $\langle C, \text{proj}_{\hat{e}_3} C \rangle$.

Figure 1A depicts the FAM coefficient maps of a short-axis slice in a normal human heart. Note that in addition to coefficient $\langle R, \text{proj}_{\hat{e}_1} R \rangle$, also known as the helix angle (HA), all the projection angles contribute to the complete description of myocardial architecture. Figure 1B shows the distribution of the FAM coefficients for the hearts imaged *in vivo* at end-diastole and end-systole. Angular variations between systole and diastole were seen for all coefficients, although the most significant changes were seen in $\langle R, \text{proj}_{\hat{e}_2} R \rangle$, $\langle C, \text{proj}_{\hat{e}_2} C \rangle$, and $\langle C, \text{proj}_{\hat{e}_3} C \rangle$ in the subendocardium. These changes depict myofiber reconfiguration in systole due to myocyte thickening, sheet sliding and sheet shearing. In addition to the 2D maps shown above, fiber tracts can be constructed by integrating \hat{e}_1 , \hat{e}_2 , or \hat{e}_3 into connected streamlines, color-coded by their projection onto any cardiac plane. In Figure 2A, \hat{e}_1 -based tracts color-coded by their projection onto the radial plane are shown. These represent myofiber tracts color-coded by the helix or spiral angle they make with the LV. Sheet tracts color coded by the projection of \hat{e}_2 onto the radial plane are shown in Figure 2B. The radial orientation of the myofiber sheets and the change in the sheet angle from the epicardium to the endocardium can be clearly seen.

Results: Figure 1A depicts the FAM coefficient maps of a short-axis slice in a normal human heart. Note that in addition to coefficient $\langle R, \text{proj}_{\hat{e}_1} R \rangle$, also known as the helix angle (HA), all the projection angles contribute to the complete description of myocardial architecture. Figure 1B shows the distribution of the FAM coefficients for the hearts imaged *in vivo* at end-diastole and end-systole. Angular variations between systole and diastole were seen for all coefficients, although the most significant changes were seen in $\langle R, \text{proj}_{\hat{e}_2} R \rangle$, $\langle C, \text{proj}_{\hat{e}_2} C \rangle$, and $\langle C, \text{proj}_{\hat{e}_3} C \rangle$ in the subendocardium. These changes depict myofiber reconfiguration in systole due to myocyte thickening, sheet sliding and sheet shearing. In addition to the 2D maps shown above, fiber tracts can be constructed by integrating \hat{e}_1 , \hat{e}_2 , or \hat{e}_3 into connected streamlines, color-coded by their projection onto any cardiac plane. In Figure 2A, \hat{e}_1 -based tracts color-coded by their projection onto the radial plane are shown. These represent myofiber tracts color-coded by the helix or spiral angle they make with the LV. Sheet tracts color coded by the projection of \hat{e}_2 onto the radial plane are shown in Figure 2B. The radial orientation of the myofiber sheets and the change in the sheet angle from the epicardium to the endocardium can be clearly seen.

Discussion: Diagonalization of the diffusion tensor produces three eigenvectors. We show here that each of these eigenvectors form projections onto the 3 cardiac planes, producing a second order fiber architecture matrix (FAM). Independent and complementary information is contained in each of the coefficients in the matrix, which can be used to create 2D maps or 3D tracts of myocardial architecture.

Conclusion: A reconfiguration of myofiber architecture, predominantly in sheet structure, occurs during systole as the heart contracts. While the HA can reveal angular differences in the orientation of myofibers across the LV wall, only by using the whole eigensystem (FAM) can the dynamics of LV contraction be fully characterized.

References: 1) Dou J *et al.*, MRM 2003; 2) Mekkaoui C *et al.*, JCMR 2012; 3) Mekkaoui C *et al.*, ISMRM 2012; 4) Osher S, JCP 1988.

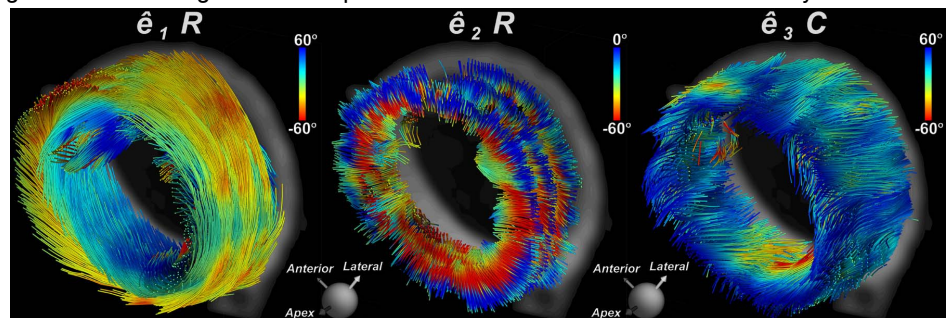


Figure 2. 3D fiber tracts of (A) $\hat{e}_1 R$, (B) $\hat{e}_2 R$ and (C) $\hat{e}_3 C$. (A) The tracts of $\hat{e}_1 R$ depict myofibers color-coded by their helix angle. The helicity (spiraling) of the fiber tracts can be clearly seen. (B) Tracts of $\hat{e}_2 R$, or myofiber sheets color-coded by their sheet angle. The radial orientation of the myofiber sheets and the transmural change in their sheet angle can be clearly seen. (C) Tracts of $\hat{e}_3 C$. The tertiary eigenvector in the LV is largely oriented from base to apex.